Indian Journal of Engineering & Materials Sciences
Vol. 32, April 2025, pp. 284-291
DOI: 10.56042/ijems.v32i02.12965

Voltage enhanced superhydrophobic ZnO micro/nanostructured coatings for anti-corrosion

Zehira Belamri[a*], Mina Boulkroune[b], Khaled Chettah[c] & Sara Benkermi[a]

[a]Phase Transformation Laboratory, Frères Mentouri Constantine 1 University, Constantine 25000, Algeria

[b]*Environmental* and *Structural Molecular Chemistry Research Unit,* Frères Mentouri *Constantine 1 University*, Constantine 25000, Algeria

[c]Mechanics Research Center (CRM), Frères Mentouri Constantine 1 University, Constantine 25000, Algeria

Received: 3 August 2024; accepted: 7 December 2024

Superhydrophobic ZnO coating has been prepared by means of electrodeposited Zn layer on aluminium substrate, followed by thermal oxidation at 500°C. In this work, the impact of applied negative potential on the physical characteristics of ZnO coatings has been studied. The samples have been investigated by field emission scanning electron microscope (FEG-SEM), energy dispersive X-ray analysis (EDX), profilometry/roughness measurements, X-ray diffraction (XRD), and Raman spectroscopy. The films wettability has been assessed via water contact angle (WCA) measurements. XRD and Raman spectroscopy analyses have confirmed the high crystallinity of elaborated ZnO thin films. FEG-SEM reveals potential-dependent morphology changes in the films. No impurity traces have been found, where EDX analysis has verified the presence only of Zn and O. Surface roughness has been observed to increase with rising negative potential from 1.356 µm for sample deposited at -10 V to 3.593 µm for sample deposited at -30 V, which has lead to an increase in contact angle values from 136.64° to 150.52°, respectively. Superhydrophobic ZnO surfaces with micro-nano topography have exhibited a hilly and valley shape. This has suggested that trapped air in surface valleys may successfully prevent corrosive wetting, such Cl^-, from accessing the denuded surface, hence offering significant corrosion protection.

Keywords: Aluminium substrate, Anti-corrosion, DC voltage, Electrodeposition, Superhydrophobic, Surface roughness

1 Introduction

The metal material has thus experienced stress corrosion cracking and corrosion fatigue, which has drastically reduced its mechanical qualities. Because of its numerous advantages, aluminium (Al) and its alloys have been widely utilized extensively in daily life, industry, aviation, and other areas. However, due to aluminium active chemical characteristics have led to damaging corrosion results[1]. Common techniques to enhance corrosion resistance have included (I) applying a corrosion–preventive material[2] and (II) surface functionalized[3]. Nevertheless, these methods have proven costly and environmentally harmful. So, it is important to develop cost-effective, simple, non-toxic, and eco–friendly surface treatments has become critical.

The electrochemical deposition approach has emerged as a promising method for manufacturing superhydrophobic surfaces, enhancing appearance, wear resistance, and corrosion resistance due to its simplicity, low cost, and ease of evolvability[4–6]. Protective coatings have played a pivotal role in safeguarding various surfaces against environmental degradation, corrosion, and fouling. Preventing frost/ice formation has been a major chalange in aeronautics, photovoltaics, and energy applications[7]. Current solutions, such as active de–icing techniques or glycol–base sprays[8], have been expensive, environmentally damaging, and difficult to impement. Passive solutions, like ice–phobic thin films, have gained traction for enabling easy ice removal with minimal adhesion forces. Superhydrophobic coatings have offered a dual adventage by combining these approaches and have attracted significant attention for their water–repellent and anti–icing properties[9].

Over the past decade, zinc oxide (ZnO) has gained promineuce as multifunctional material for the development of hydrophobic[10-14]or superhy drophobic[15] coatings due to its abundance, low cost, and tunable properties. Micro/nanostructures have further enhanced superhydrophobicity by creating air–trapping topographies[16]. The application of DC voltage during synthesis has provided a means to tailor coating morphology and performance.

In this study, protective superhydrophobic ZnO coatings have explored and the effects of DC voltage

*Corresponding author (E-mail: belamri.zehira@umc.edu.dz)

on their properties have investigated. Through synthesis optimization and experimental analysis, the relationship between processing parameters and the properties of these coatings have clarified. The insights have advanced the understanding of superhydrophobicity and have supported the development of durable, functional coatings.

2 Materials and Methods

2.1 Samples preparation

Before deposition of Zn layers, the aluminium alloy substrates were polished with silicon carbide paper of 600 grains/cm^2 until it takes on a flat with 2 mm thickness, and then washed ultrasonically with distilled water and methanol for 15 minutes, respectively, and then dried.

An aqueous solution of dehydrated zinc acetate (Zn $(CH_3COO)_2$-$2H_2O$) precursor was prepared using distilled water to make an aqueous solution with 0.2 M. Aluminium (cathode) and Pt (anode) were vertically immersed in the solution (1.5 cm apart).A negatives DC voltages of -10, -20, and -30 V were applied for 15 minutes. The electrolyte temperature was maintained constant at 50°C throughout the process to activate chemical reactions. In order to obtain hydrophobic and superhydrophobic properties on aluminium surfaces, the electrodeposited Zn layers were further thermally oxidized at 500°C for 5 hours. Our earlier research[10] made it evident that temperatures below 500°C are not high enough to produce a full ZnO complex, which is necessary to guarantee the entire oxidation of Zn.

2.2 Characterization

PANALYTICAL empyrean diffractometer (XRD, λ_{Cu}= 1.540 Å) is used to determine the crystallographic properties of the as-prepared thin films. The data from XRD was analyzed using X'Pert High Score software. A monochromatic light source measuring 473 nm was used to measure the Raman spectra on a HORIBA LabRAM HR Evolution spectrometer at ambient temperature. In this work, we compared the vibration modes of the analyzed samples using zinc oxide (ZnO) powder which obtained commercially from Fluka Analytical. For material characterization, we employed a JEOL FEG JSM-7100F field emission scanning electron microscope with integrated energy-dispersive X-ray spectroscopy (FEG-SEM/EDS) to examine surface morphology and elemental composition. Film thickness and roughness measurements were conducted using a PCE-RT 1200 profilometer Tester. Water contact angle measurements were employed to characterize the surface wettability of the elaboratecd ZnO thin films. This measurement has been used by means of a light source type LEYBOLD (6 V, 30 W) for lighting and projecting the drop's image onto the sample, together with a projection lens that allowed the image to be magnified onto a transparent screen of dimensions 30x30 cm^2.

Potentiodynamic polarization curves were recorded by an electrochemical workstation (GAMRY Instruments, Reference 3000) in 3.5 wt% NaCl solution for 10 days immersion at room temperature. Potentiometric polarization curves were obtained with at a sweep rate of 10 mV/s in the Tafel model from -1600 mV to -500 mV.

3 Results and Discussion

3.1 Structural studies

Figure 1 highlights the findings of a thorough examination of the crystallized phases of the synthesized ZnO samples. This analysis was conducted using an X-ray diffraction pattern at room temperature. The ZnO thin films structure wasdetermined by comparing their spectrum data to known databases, specifically ICSD card N°: 00-036-1451.

The Wurtzite hexagonal structure was confirmed after treatment at 500°C for 5 h of electroplating Zn layers. This was evident from the distinct diffraction peaks observed at specific angles; 31.770°, 34.422°, 36.253°, 47.539°, 56.603°, 62.864°, 67.974° and 69.275°. These angles correspond to the (100), (002),

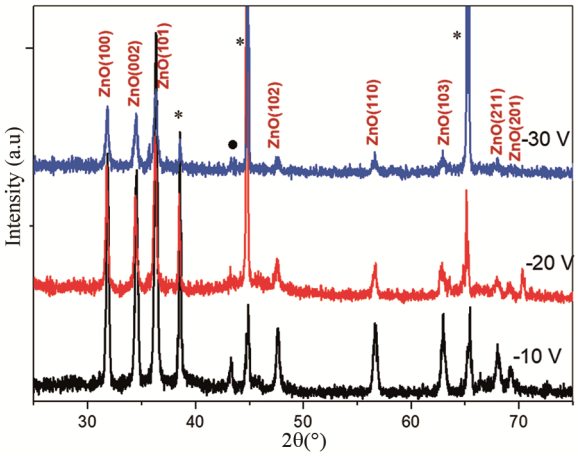

Fig. 1 — XRD spectra of elaborated ZnO thin films with different applied negative voltage (-10 V, -20 V, and -30 V) and annealed 5 h at 500°C (*: Al and •: Zn).

Table 1 — Values of crystallite sizes, e_{zz}, σ, and δ as a function of applied negative potential for elaborated ZnO thin films annealed 5 h at 500°C.

Applied DC voltage (V)	2θ (°) of (101) peak	FHWM (°)	Crystallites size D (nm)	e_{zz}(%)	σ (GPa)	Dislocation density δ x 10^{14} (ligne/m^2)
-10	36,3409	0,3070	28	-0,7551	1,7594	1,2358
-20	36,2628	0,2303	38	-0,4003	0,9327	5,4961
-30	36,3164	0,3070	28	-0,2854	0,6651	1,0509

(101), (102), (110), (103), (211) and (201) lattice planes of the Wurtzite hexagonal structure, as shown in Fig. 1. The high intensity of (100), (002), and (101) peaks, which characterizes all samples, indicates that the products have a desirable crystalline quality and high purity[17,18]. For all elaborated ZnO thin films, growth is evident along the (101) plane, which exhibits the highest intensity. Therefore, the difference between the applied negative potentials has no effect on the crystallographic orientation of ZnO growth on aluminium substrates.

The crystallites size was calculated by using Scherer equation[19] using the Full Width at Half Maximum (FWHM) of the highly oriented peak (101) located around 36.2 ° in the XRD spectrum, eq. 1:

$$D = \frac{0.9\lambda}{\beta \cos\theta} \quad \ldots(1)$$

Where, λ, θ, and β are the X-ray wavelength (0.1540 nm), Bragg diffraction angle, and FWHM, respectively. The size of crystal size as a function of applied negative potential is summarized in Table 1.

The experimental results demonstrate that the crystallite size is nanometric, whereas the samples elaborated with -10 V and -30 V have a low values. A possible explanation for this difference is as follow: at low voltages -10V, the nucleation rate is slower, allowing a more regular growth of crystallites which remain small. At higher voltages -30V, supersaturation is maximum the nucleation rate is very fast, which limits the crystallites size that remains small. It is found that the high supersaturation rates can favor smaller crystal sizes with broad size distributions[20]. At the intermediate voltage -20V, the nucleation rate is higher, but the supersaturation may not yet be sufficient to completely inhibit the nuclei growth. This favors the growth of crystallites, which reach a larger size.

XRD allows evaluation of internal stresses in ZnO films through diffraction peak position analysis. The biaxial stress (e_{zz}) along the c-axis direction perpendicular to the substrate is calculated from the following relationship[21]:

$$e_{zz} = \frac{C_{film} - C_0}{C_0} \times 100 \quad \ldots(2)$$

Where c_{film} is the lattice parameter of the elaborated thin film and $c_0$isthe lattice parameter of the unconstrained thin film (c_0 = 0.5213 nm). We can confirm the type of stress by studying the sign of the e_{zz} parameter. In this present work, the e_{zz} values represented in Table 1 are negative, which confirms that this film undergoes a compressive stress parallel to its growth direction. The residual stress parallel to the thin film surface is expressed as follows[22]:

$$\sigma = \frac{2C_{13}^2 - C_{33}(C_{11}+C_{12})}{2C_{13}} \text{ x } \frac{C_{film} - C_0}{C_0} \quad \ldots(3)$$

With c_{ij} is the elastic constant for a monocrystalline structure of ZnO (c_{13} = 104.2 GPa, c_{33} = 213.8 GPa, c_{11} = 208.8 GPa and c_{12} = 119.7 GPa[23]):

$$\sigma(GPa) = -233 \text{ x } e_{zz} \quad \ldots(4)$$

Analysis revealed an inverse correlation between biaxial stress (e_{zz}) and residual stress, demonstrating opposing orientations in the film-substrate interface plane[24]. The calculated (σ) values of the elaborated samples at different voltages are presented in Table 1. The positive sign of all measured values confirms that the synthesized ZnO thin films are under traction stress oriented perpendicular to the c-axis. This stress variation correlates directly with the applied negative voltage, suggesting a voltage-dependent stress modulation mechanism. The sample prepared with -30 V has a low value of residual stress and a low value of dislocation density (δ) indicates the presence of fewer defects in the deposited ZnO thin film. So, this voltage corresponds to the best crystallization of the ZnO hexagonal phase.

In this work, Raman spectroscopy was utilized to analyze the structural characteristics of the elaborated ZnO thin films with different applied negative potentials. The Raman signals are quite sensitive to both the structure and defects of the crystal. Determining the various phases of the material under study is a result of identifying the various crystal lattice vibration modes.

The obtained spectrum (Fig. 2) of elaborated samples with different applied negative potentials appears akin to that of bulk ZnO[11]. It comprises four peaks that correspond to the E_2^{low}, E_2^{high}-E_2^{low}, E_2^{high}, and E_1(LO) modes of the ZnO phonons found in the hexagonal structure.The prominent peak, identified as E_2^{high} at around 441 cm^{-1}, was detected and is recognized as the Raman-active optical phonon mode. This mode is related to the vibration of the oxygen atom sublattice in the Wurtzite hexagonalZnO crystal[25,26]. The high intensity of this peak reflects the crystallization quality of the hexagonal WurtziteZnO structure[27-29].The peak at approximately 102 cm^{-1}, referred to as E_2^{Low}. This peak is connected to the vibration of the zinc atom lattice. The peak at 336 cm^{-1} corresponds to the second-order Raman spectrum, originating from the phonons E_2^{high} - E_2^{Low} at the zone boundary[27,30] resulting from the multiphonon process[31].Other, heightened peaks were identified on the Raman spectrum that correspond to the E_1(LO) modes. These modes are known to be Raman-active and are specific to the hexagonal WurtziteZnO structure, with a frequency of approximately 587 cm^{-1}, resulting from impurities and flaws in the formation process, such as the presence of oxygen vacancies.

According to the results of this examination, there are no alterations in the Raman spectra when the voltage was increased. Consequently, the increase in applied voltage does not have an effect on the vibration mode of the elaborated ZnO. This could be attributed to a few potential factors: ZnO might have achieved a stable crystal structure after a specific period of annealing time and voltage, implying that further increments in these factors will not yield noteworthy modifications in the crystal structure[31].

3.2 Morphological studies

The surface morphology of ZnO thin films obtained with different applied negative voltages is displayed in Fig. 3 (a-b). These images reveal alterations in the surface morphology of the studied samples with an increase in applied negative voltage. In the domain of micrometrics, the sample deposits at -10 V (Fig. 3(a)) display vertical micro sheets with a needle-like formation.

The FEG-SEM image of the sample deposits at -20 V (Fig. 3 (b)) clearly illustrates the formation of micrometer structure covered with nanometric compact grains distributed uniformly on the surface. While the sample deposits at -30 V (Fig. 3 (c)) reveals the presence of both micro and nanostructures

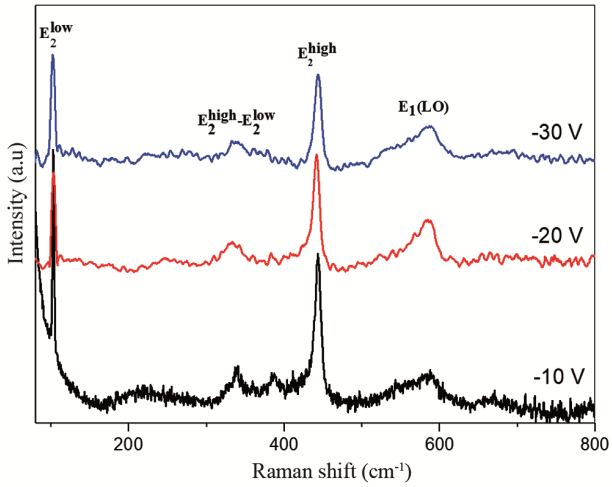

Fig. 2 — Raman spectrum of elaborated ZnO thin films with different applied negative voltage (-10 V, -20 V, and -30 V) and annealed 5 h at 500°C.

resembling a flower (The hill-and-sphere dual-scale topography, clearly visible in magnified SEM images, creates the necessary surface roughness for superhydrophobicity, with the spherical ZnO nanostructures providing nanoscale texturing atop micrometer-scale hills). The ZnO nanostructures begin shaped uniformly as cubes, with a few appearing spherical[32]. This material is known for its significant porosity[24]. There are numerous layers of ZnO present on the substrates, as shown by the varying brightness levels of the grains. The upper layer of the thin films is represented by the brighter grains, and the lower layer is represented by the obscurer grains (image inset in Fig. 3 (c)).

Energy-dispersive X-ray spectroscopy (EDX) was used to verify the chemical composition of the ZnO films (Fig. 3). The analysis confirmed the exclusive presence of zinc (Zn) and oxygen (O), with no detectable elemental impurities, indicating high-purity ZnO formation.

3.3 Wettability study of the elaborated ZnO thin films

Measurements of contact angles can be utilized to demonstrate hydrophobiccharacteristics[33]. It is observed that the aluminium surfaces did not show the hydrophobic or superhydrophobic properties as we observed in the case of ZnO coated aluminium surface. The applied negative potential has an effect on the contact angle values of the studied samples (Fig. 4). The greatest value of the contact angle is obtained after a treatment of 5 hours at 500°C of the elaborated layers, which achieved the maximum of 150.52° for the sample prepared with -30V. The obtained superhydrophobicity

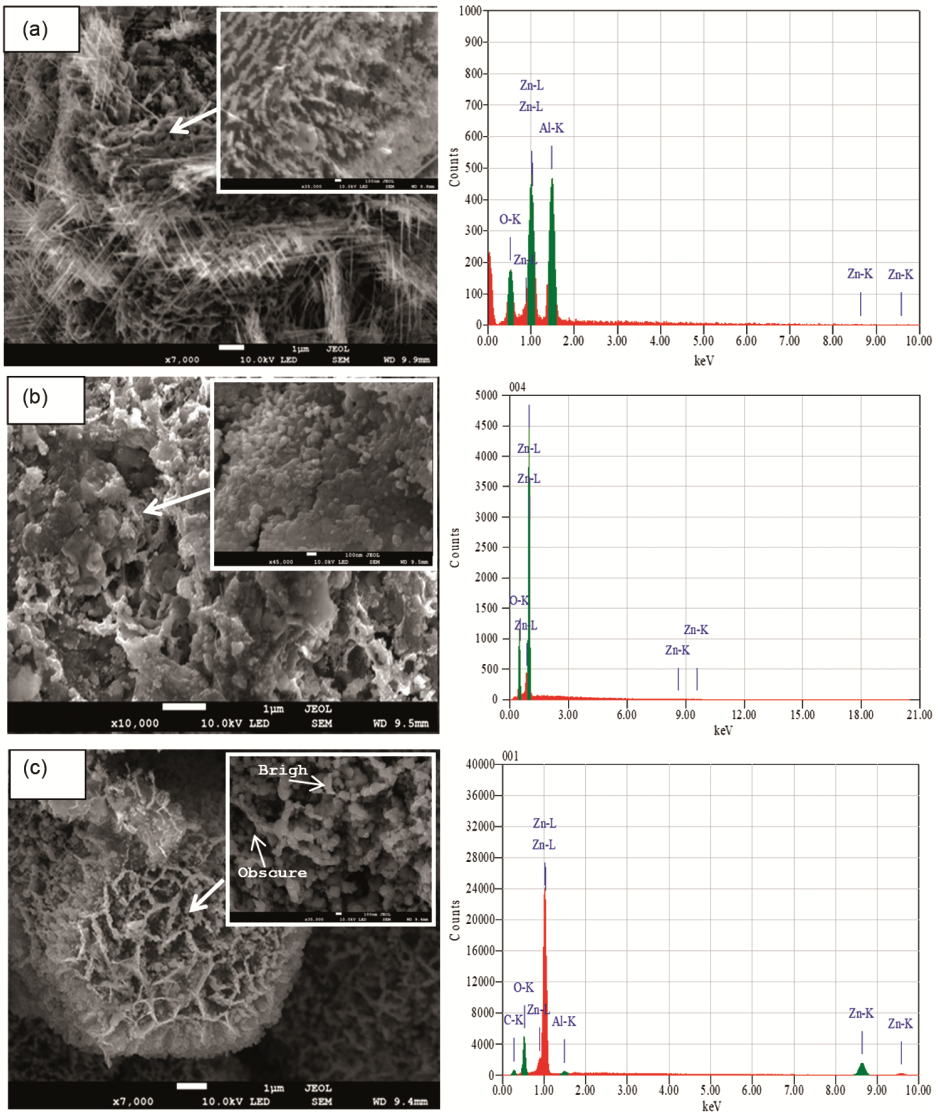

Fig. 3 — FEG-SEM images of ZnO thin films deposited on aluminium substrates at different applied negative voltage then annealing 5 h at 500°C: (a) -10 V, (b) -20V, and (c) -30 V.

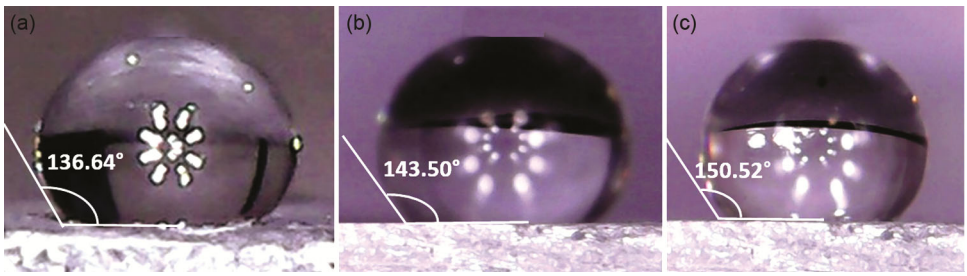

Fig. 4 — WCA measurements showing potential-dependent wettability of ZnO films electrodeposited on aluminium 5h at 500°C under varying applied negative potential (a) -10 V, (b) -20V, and (c) -30 V.

can be explained by the effect of the surface roughness of the elaborated samples. In this work, the surface roughness increases with the increase in the applied negative potential from 1.356 µm for sample deposited at -10 V to 3.593 µm for sample deposited at -30 V, which leads to an increase in contact angle values from 136.64° to 150.52°, respectively (Table 2). Higher contact angles are produced by

rough surfaces because they have a tendency to trap air pockets that prevent the liquid from spreading.

Previous studies have established that surface roughness significantly enhances hydrophobicity by promoting the Cassie-Baxter state, where the liquid droplet rests on composite solid-air interfaces rather than fully penetrating surface asperities. This phenomenon creates trapped air pockets within surface grooves, effectively increasing the observed contact angle[34]. A possible explanation for the increase in surface roughness with increasing applied negative voltage may be that the increasing voltage causes an increase in the electric field strength in the electrolyte solution, which helps force the materials with an electrochemical reaction to be deposited on the cathode. However, when the applied negative voltage is -30 V, it can be observed that some external coating material started to fall off from the cathode in the last step of the electrodeposition process,which explains the decrease in the thickness of the studied samples with increasing voltage (Table 2).

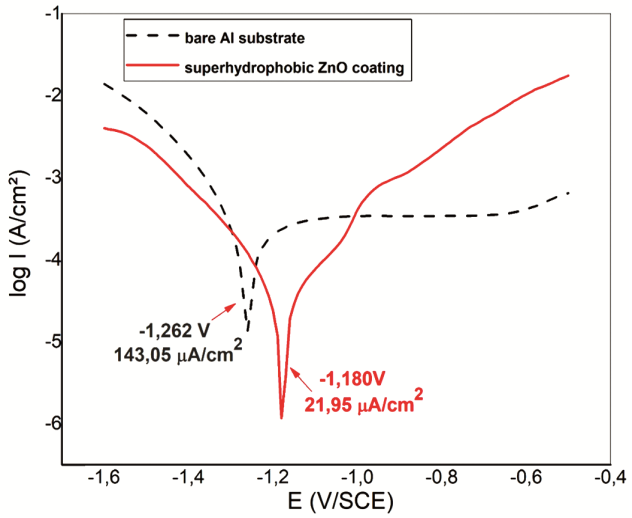

Fig. 5 — Potentiodynamic polarization curves of the aluminium electrodes with and without the superhydrophobic ZnO coating for 10 days in 3.5% NaCl solution at room temperature with 10mV. s^{-1}.

Table 2 — Values of thickness, roughness and contact angle as a function of applied negative potential for elaborated ZnO thin films annealing 5 h at 500°C.

DC (V)	Thickness (µm)	Roughness (µm)	Contact Angle (degree)
-10	18.00	1.356	136.64
-20	13.50	2.009	143.50
-30	8.33	3.593	150.52

3.4 Potentio-dynamic polarization measurements

Corrosion potential (E_{corr}) and corrosion current density (I_{corr}) are the two characteristics of polarization curves that indicate a surface's protective qualities. As is often known, a high level of corrosion resistance is indicated by a decrease in I_{corr} and an increase in E_{corr}. I_{corr} is the only source of corrosion rate information.

Figure 5 shows that the anti-corrosion properties were evaluated by potentiodynamic polarization. The corrosion potential and corrosion current density were found by using the intersection of the two slopes[35] using Tafel extrapolation. A larger E_{corr} indicates that the kinetics of corrosion will be governed by the current density, but that corrosion activation will be more challenging.

Tafel analysis of the polarization curves identified three key electrochemical parameters: corrosion potential (E_{corr}), corrosion current density (I_{corr}), and polarization resistance (R_p). These fundamental metrics, which quantify the material's corrosion behavior, are systematically presented in Table 3. The anodic and cathodic curves were extrapolated to determine E_{corr} and I_{corr} from the crossing sites. The following Stern-Geary equation[36] was used to calculate the polarization resistance (Rp):

$$R_p = \frac{\beta_a \beta_c}{2.3\, I_{corr}(\beta_a \beta_c)} \quad \ldots (5)$$

Where β_a and β_c are the anodic and cathodic Tafel slopes, respectively.

The aluminium substrate exhibited a corrosion current density (I_{corr}) of 143.05 µA/cm^2 and a polarization resistance (Rp) of 320.75 Ω.cm^2, while the I_{corr} and Rp of the same substrate coated with superhydrophobicZnO thin films were found to be only 21.95 µA/cm^2 and 1208.27 Ω.cm^2 respectively. It has been proved that larger polarization resistance and a lower corrosion current density indicate excellent

Table 3 — Fit parameters for Tafel analysis of potentiodynamic polarization test of the aluminium electrodes with and without the superhydrophobic ZnO coating for 10 days in 3.5% NaCl solution at room temperature with 10 mV. s^{-1}.

Sample	E_{corr}(V/ECS)	I_{corr} (µA/cm²)	β_a (V/decade)	β_c (V/decade)	C_R (mpy)	R_p(Ω/cm^2)
Bare Al substrate	-1.262	143.05	617.2 10^{-3}	127.3 10^{-3}	190.3	320.75
Al substrate with superhydrophobic ZnO coating	-1.180	21.95	139.5 10^{-3}	108.4 10^{-3}	17.87	1208.27

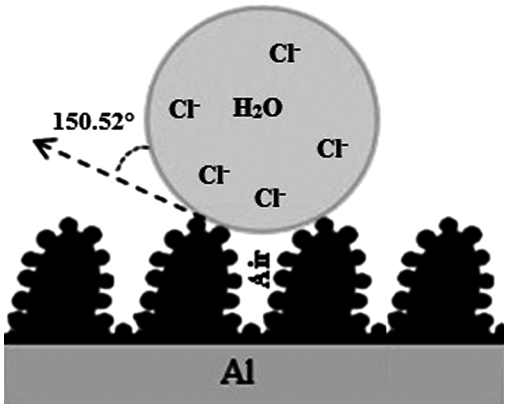

Fig. 6 — Schematics describe the supposed corrosion resistance mechanism of the elaborated superhydrophobic ZnO coating.

anti-corrosion properties of the superhydrophobic ZnO coating. The corrosion rate is determined by the corrosion current density, which is inversely correlated with polarization resistance.

3.5 Correlation between the superhydrophobicity, the surface morphology and anti-corrosion property of studied sample

Figure 6 shows the schematic illustration of the possible conformation of the surface microstructure with the superhydrophobic coating at the air/layer interface as well as the water droplet in contact with this surface. Rough surfaces on both the micro- and nanoscale (referred to as "micronanobinary structures"[37]) are the most promising for reaching the superhydrophobic surfaces. Previous studies[37] have established that surface wettability can be significantly enhanced by optimizing surface roughness within a specific micro/nanoscale range. This effect arises from air entrapment in surface asperities, which reduces the effective liquid-solid contact area. Several previously published works on superhydrophobic surfaces made using water[38,39] highlight the critical role that the coexistence of low surface energy coating and surface roughness (micro-nanostructure) plays for surfaces that exhibit superhydrophobicity.

According to FEG-SEM observation of the surface of the sample prepared with (-30) V, the micro- and nano-scale hills structure present at the aluminium surface. Thus, nanostructured ZnO covering the micro roughnesses of the zinc layer perfectly respects Cassie Baxter's model. A great amount of air is imprisoned in the solid–liquid contact area at the hills superhydrophobic surface which covered by a large number of uniform spherical ZnO nanostructures of about 100 nm in size, as shown in the magnified images (Fig. 3 (c)). Water droplets are unable to enter the air-held gaps in the abrasive, superhydrophobic aluminium surface due to the air's water-repellency. Consequently, the superhydrophobic surface develops an "air cushion," and the droplet encloses tiny air-filled cavities under it, decreasing the area of the water/surface interface on a microscopic scale[40]. Thus, it would be very difficult for the corrosive ion to close and penetrate into the superhydrophobic surface due to the protection provided by the "air cushion" on the superhydrophobic aluminium surface. Additional important reason why the modified surface can improve the anticorrosion of aluminium is ‘capillarity’. When a vertical cylindrical tube is immersed in a liquid, the liquid is deceases if the tube is superhydrophobic.

4 Conclusion

Superhydrophobic ZnO coatings were prepared on aluminium substrates by the electrodeposition process. The superhydrophobicity of these coatings can be inferred from the wettability measurement that the hydrophobicity of such coatings increases with increasing applied voltage. By means of the "air cushion effect," the superhydrophobic surface plays a crucial role in preventing the corrosion response. The hill and valley morphology of superhydrophobic ZnO surfaces exhibiting micro-nano topography; the air trapped in the “valleys” can prevent corrosive fluids, e.g. Cl^-, from effectively reaching the denuded surface, thus providing good corrosion protection.

References

1 Du X Q, Liu Y W & Chen Y, *Appl Phys A,* 127 (2021) 1.
2 Shuwei L, Xinming Z, Xiaodong Y, Xianli L, Zhuojuan Y & Ying Z, *Mater Res Express*, 9 (2022) 026520.
3 Zheng S, Li C, Fu Q, Hu W, Xiang T, Wang Q, Du M, Liu X & Chen Z, *Mater Des,* 93 (2016) 261.
4 Tam J, Palumbo G & Erb U, *Mater,* 9 (2016) 1.
5 Fateh A, Aliofkhazraei M & Rezvanian AR, *Arab J Chem,* 13 (2020) 481.
6 Xu G, Wang K, Dong X, Yang L, Ebrahimi M, Jiang H, Wang Q & Ding W, *J Mater Sci Technol,* 21 (2021)12.
7 Dhyani A, Choi W, Golovin K & Tuteja A, *Mater,* 5 (2022) 1423.
8 Li T, Pablo F. Ibáñez I, Håkonsen V, Wu J, Xu K, Zhuo Y, Luo S, He J & Zhang Z, *ACS Appl Mater Interfaces*, 12 (2020) 35572.
9 Cannio M, Boccaccini D N, Caporali S & Taurino R, *Clean Technol, 6* (2024) 299 .
10 Belamri Z, Darenfad W & Guermat N,*J. Nano- Electron Phys*, 15 (2023) 1.

11 Belamri Z, Bouamaza L & Boudjadar S, *Physica Scripta*, 98 (2023) 1.
12 Belamri Z, Darenfad W & Guermat N, *Eur Phys J Appl Phys*, 99 (2024) 10.
13 Belamri Z, Mermoul N & Hamana D, *Acta Phys Pol A*, 145 (2024) 301.
14 Belamri Z, *Springer Proceedings in Materials*, 45 (2023) 125-131, 9–10 October, Algeria.
15 Mardosaitė R, Jurkevičiūtė A & Račkauskas S, *Cryst. Growth Des* 21: 4765.
16 Tang Z Q, Tian T, Molino P J, Skvortsov A, Ruan D & Li Y (2024), *Adv Sci,* 11 (2021)1.
17 Nagarajan K, Anoopsirishkataru B, Sravani N & Vigneshwari T, *Open Nano*, 3 (2018) 48.
18 Byeon H, Sreenivasan V S, Krishna A R, Thosar C P, Randhavane S B, Baghel D S & Sunil J*, Bull Chem Soc Ethiop,* 38 (2024) 417.
19 Kenanakis G, Stratakis E, Vlachou K, Vernardou D, Koudoumas E & Katsarakis N, *Appl Surf Sci,* 254 (2008) 5695.
20 Ouda A, Bajon-Fernandez Y & McAdam E, *J Membr Sci,* 691 (2024) 1.
21 Karyaoui M, Jaballah A B, Mechiak R & Chtourou R, *IOP Conf Ser Mater Sci Eng,* 28 (2012) 1.
22 Tüzemen E S, Eker S, Kavak H & Esen R, *Appl Surf Sci,* 255 (2009) 6195.
23 Jacob A A, Balakrishnan L, Meher S, Shambavi K & Alex Z, *J Alloys Compd,* 695 (2017) 3753.
24 Srinivasulu T, Saritha K & Ramakishna R K T, *Mod Electron Mater,* 3 (2017) 76.
25 Lima L, Caldas Lucas de S, Alí A, Barreto J, Freitas R, Mazzarella A, Felix G, Carozo V & Stavale F, *Surf Sci,* 704 (2021) 1.
26 Prasad S, Bansal S & Pandey S P, *Mater Today,* 49 (2020) 3022.
27 Dasi G, Lavanya T, Suneetha S, Vijayakumar S, Shim J J & Thangaraju K, *Spectroc Acta A,* 265 (2022) 1.
28 Thiruvengadathan R, Dhua S, Rani S, Mathai C J, Bai M, Gangopadhyay K & Gangopadhyay S, *Mater Adv*, 3 (2022) 5383.
29 Silambarasan M, Saravanan S & Soga T, *J Surf Sci Nanotechnol,* 12 (2014) 283.
30 Kasirajan K, Chandrasekar L B, Maheswari S, Karunakaran M & Sundaram P S, *Opt Mater*, 121 (2021) 1.
31 Khan A, *J Pak Psychiatr Soc*, 4 (2010) 5.
32 Hutera B, Kmita A, Olejnik E & Tokarski T, *Arch Metall Mater*, 58 (2013) 489
33 Suci E & Suryani I, *J Phys Conf Ser*, 1093 (2018) 1.
34 Cassie A B D & Baxter S, *Trans Faraday Soc*, 40 (1944) 546.
35 Xiong J, Sarkar D K & Chen X G, *Appl Surf Sci,* 407 (2018) 361.
36 Singh A K, Drunka R, Iesalniece P, Blumbergs I, Steins I, Eiduks T V, Iesalnieks M & Savkovs K, *Surf,* 6 (2023) 364.
37 Zhang J, Huang W & Han T, *Langmuir*, 22 (2006) 2946.
38 Huang Y, Sarkar D K & Chen X-G, *Nano-Micro Lett,* 3 (2011) 160.
39 Sarkar D K, Farzaneh M & Paynter R W, *Mater Lett,* 62 (2008) 1226.
40 Feng L, Che Y, Liu Y, Yan Z, Wang Y & Qiang X, *Surf Interface Anal,* 48 (2016)1320.